Available online at www.sciencedirect.com
SCIENCE DIRECT
Polymer 46 (2005) 8641–8660
polymer
www.elsevier.com/locate/polymer

Rheological characterization of polystyrene–clay nanocomposites to compare the degree of exfoliation and dispersion

Jin Zhao[a,*], Alexander B. Morgan[b,1], Joseph D. Harris[c]

[a]*Materials Science, Materials Research Group, Corporate R&D, The Dow Chemical Company, Midland, MI 48674, USA*
[b]*Chemical Sciences, Inorganic Materials Group, Corporate R&D, The Dow Chemical Company, Midland, MI 48674, USA*
[c]*Analytical Sciences, Corporate R&D, The Dow Chemical Company, Midland, MI 48674, USA*

Received 16 November 2004; received in revised form 18 April 2005; accepted 20 April 2005
Available online 15 August 2005

Abstract

Polymer–clay nanocomposites are of great interest due to their improvement in certain material properties relative to virgin polymer or conventional composites. For example, compared to conventional materials, Nylon 6/montmorillonite nanocomposites demonstrated significant improvements, including high strength, high modulus and high heat distortion temperature. Because viscoelastic measurements are highly sensitive to the nanoscale and mesoscale structure of polymeric materials, when combined with X-ray scattering, electron microscopy, thermal analysis, and mechanical property measurements, they will provide fundamental understanding of the state and mechanism of exfoliation of the layered silicate (clay) in a polymer matrix. In addition, understanding rheological properties of polymer nanocomposites is crucial for application development and understanding polymer processability.

The objective of this research is to develop a rheological technique to analyze the clay morphology in nanocomposite. Previous work has demonstrated the utility of the rheological technique to differentiate (qualify) the degree of exfoliation/dispersion. This report utilizes findings from the earlier work to further map out the structure-rheological response of polystyrene nanocomposites with various composition, clay types, and dispersion; and to quantify the key parameter that dominates the characteristic rheological response. This report explored a series of polystyrene (PS)–clay nanocomposites with 1,2-dimethyl-3-*n*-hexadecyl imidazolium (DMHDI) organically modified clays. These PS nanocomposites investigated here demonstrated a change of pattern in dynamic mechanical spectrum, as a function of the degree of exfoliation, from typical polymer response to a terminal response of [$G' \sim \omega$, $G'' \sim \omega$], then to a pattern with double crossover frequencies, and finally to a solid-like response with $G' > G''$ in all frequency ranges. We showed that the number of particles per unit volume is a key factor determining the characteristic response of nanocomposites.

In addition, the rheological response of PS–clays nanocomposite made from DMHDI modified clay combined with high-energy sonication (characterized as exfoliated by XRD and TEM) was compared with that of nanocomposites made by dimethyl, benzyl hydrogenated tallow (2MBHT) modified clay. We found that PS nanocomposites made by DMHDI-modified clay with high-energy sonication are better dispersed than the nanocomposites made previously using 2MBHT-modified clay. We also showed that the glass transition temperatures were not very sensitive to the degree of dispersion.

The key finding of this research is that rheological measurements are complimentary to traditional polymer nanocomposite analysis techniques, and they may also serve as an analytical tool by itself (under appropriate conditions), now that some fundamental behavior has been identified.

Keywords: Nanocomposite; Rheology; Polystyrene

1. Introduction

Polymer nanocomposites are of great interest due to improvement in certain material properties relative to virgin polymer or conventional composite materials. When compared to conventional materials, polymer–clay nanocomposites have demonstrated improvements in mechanical, conductive, thermal, and flammability properties. It is

* Corresponding author. Tel.: +1 989 636 4828; fax: +1 989 636 2224.
E-mail address: jzhao@dow.com (J. Zhao).
[1] Present address: University of Dayton Research Institute (UDRI), Dayton, OH 45469.

0032-3861/$ - see front matter © 2005 Elsevier Ltd. All rights reserved.
doi:10.1016/j.polymer.2005.04.038

Table 1
Formulation and properties of PS + DMHDI–clay nanocomposites

Sample formulation	Synthesis method	Sample ID	XRD (nm)		TEM dispersion
			d(100) measured	*d*(100) change	
PS + 1.45 wt% DMHDI-MMT	Solvent, no sonication	PSN-1	3.24	1.3	Intercalated
PS + 1.48 wt% DMHDI-FSM	Solvent, no sonication	PSN-2	3.1	0.94	Intercalated
PS + 3.63 wt% DMHDI-MMT	Solvent, no sonication	PSN-3	3.14	1.2	Intercalated
PS + 3.72 wt% DMHDI-FSM	Solvent, no sonication	PSN-4	2.94	0.78	Intercalated
PS + 1.45 wt% DMHDI-MMT	Solvent + sonication	PSN-5	3.23	1.29	Exfoliated
PS + 1.48 wt% DMHDI-FSM	Solvent + sonication	PSN-6	3.28	1.12	Intercalated
PS + 3.63 wt% DMHDI-MMT	Solvent + sonication	PSN-7	3.37	1.43	Exfoliated
PS + 3.72 wt% DMHDI-FSM	Solvent + sonication	PSN-8	3.17	1.01	Exfoliated

The *d*(100) difference numbers are obtained by subtracting the *d*(100) of the DMHDI-MMT and DMHDI-FSM base clays, which have *d*-spacings of 1.94 and 2.16 nm, respectively.

rare that a technology can improve both flammability and mechanical properties for a polymer, as the usual phenomena are for one property to be gained at the expense of another. Such improvements will likely continue to have major positive impacts in the materials industry, as there are commercial polymer clay nanocomposites in use today [1,2]. Because viscoelastic measurements are highly sensitive to the nanoscale and mesoscale structure of polymeric materials, they can provide a fundamental understanding of the degree of layered silicate (clay) exfoliation in a polymer matrix when combined with X-ray scattering, electron microscopy, thermal analysis, and mechanical property measurements. In addition, understanding the rheological properties of polymer

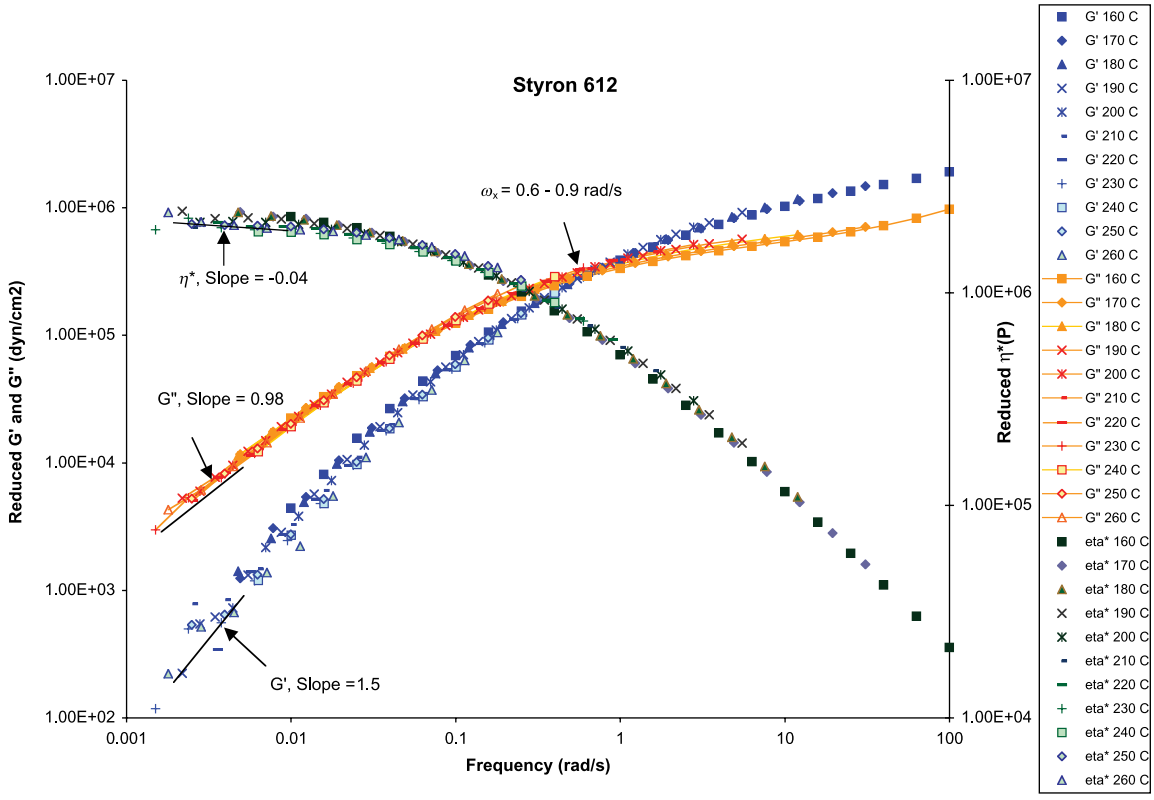

Fig. 1. Reduced frequency dependence of storage modulus, G', loss modulus, G'', and complex viscosity, η^* of pure PS, STYRON* polystyrene 612.

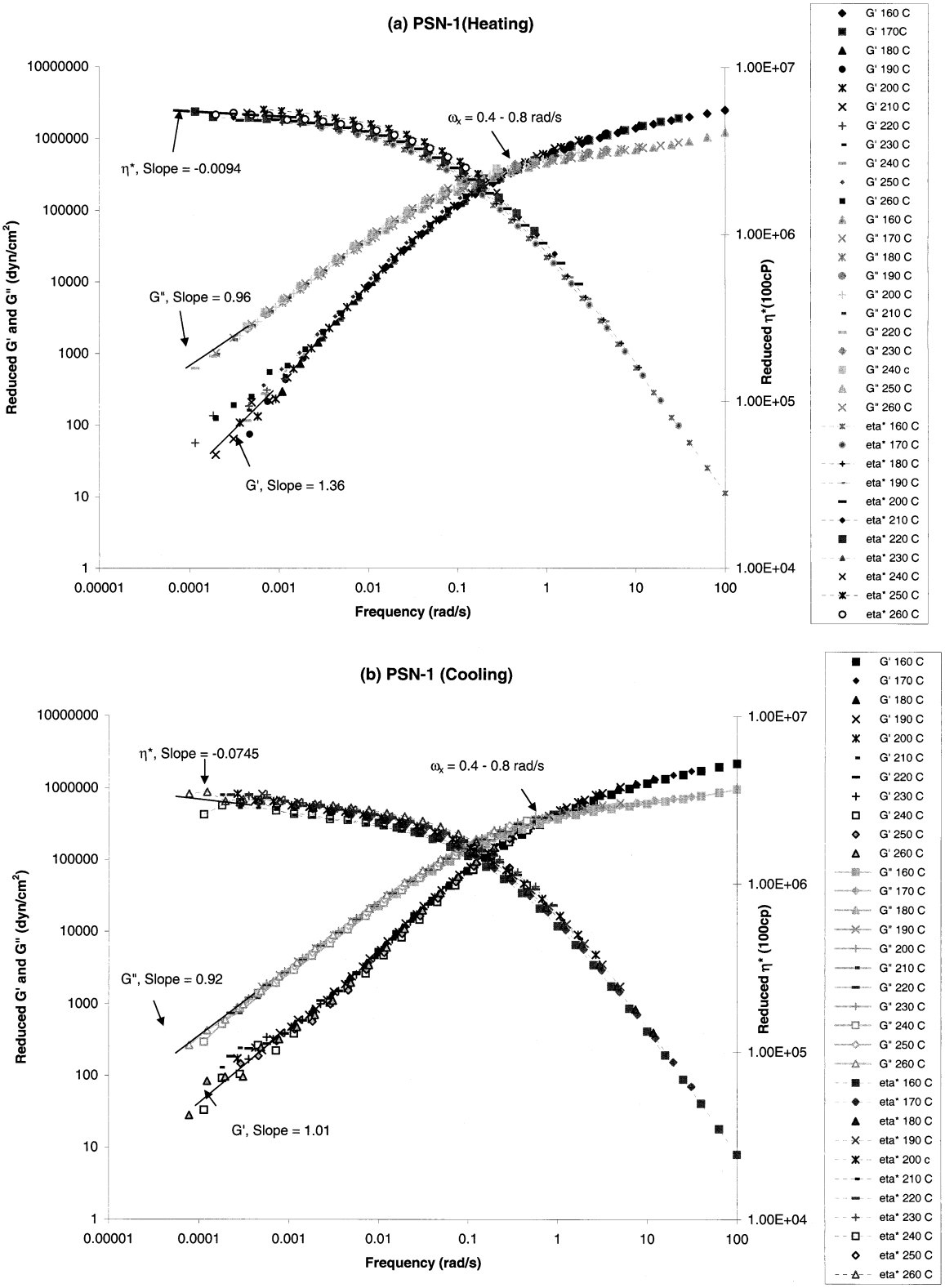

Fig. 2. Reduced frequency dependence of storage modulus, G', loss modulus, G'', and complex viscosity, η^* of PS + 1.45 wt% DMHDI-MMT, no sonication (PSN-1). Master curve (a) was obtained by heating the sample from 160 to 260 °C. Master curve (b) was obtained by annealing the sample at 260 °C and then cooling the sample down from 260 to 160 °C.

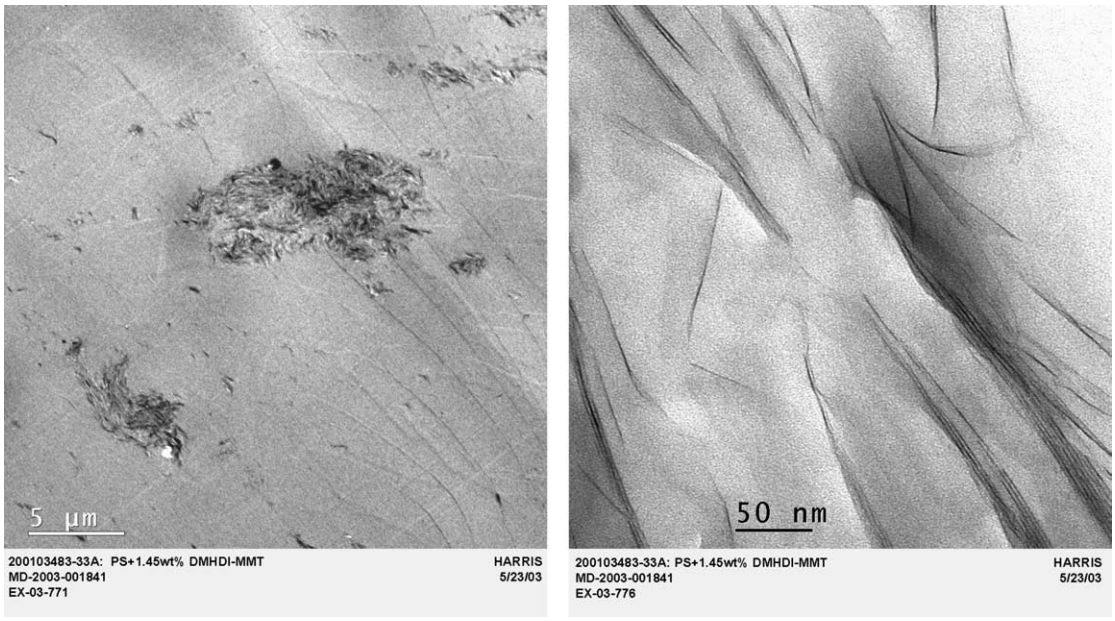

Fig. 3. TEM images of PS + 1.45 wt% DMHDI-MMT (PSN-1), no sonication.

nanocomposites is crucial for application development and understanding polymer processability [3].

The degree of intercalation, exfoliation, and dispersion has been traditionally characterized by X-ray diffraction (XRD) and transmission electron microscopy (TEM). While both are effective tools, they are limited in that they only probe a small volume of the sample and can be costly for routine characterization of nanocomposites. Further, neither XRD nor TEM alone can accurately describe the levels of clay dispersion and polymer nanocomposite structure. Multiple techniques (usually XRD, TEM combined with another technique) are needed for nanocomposite analysis to properly understand what type of nanocomposite has been made, as no one technique can adequately describe the system [4,5]. Melt rheology could quantify via a global average of the degree of intercalation/exfoliation/dispersion across the whole nanocomposite test specimen, which is usually around 2 g of sample. It is has the potential to be ambiguous than other techniques in quantifying exfoliation/dispersion and in probing percolation threshold. In addition, it is easier to perform than TEM and XRD thereby opening up the possibilities of performing routine studies to better understand the influence of material options and processing conditions for improving nanocomposite exfoliation/dispersion. It is important to note that the for the possibility of quantification to exist, the measured rheology will need to be 'calibrated/correlated' a known nanocomposite dispersion, which would come from traditional nanocomposite analysis (XRD, TEM, etc). A wealth of experimental studies on the interrelationship between rheological properties and nanocomposite morphologies has already been accumulated [6–17]. However, the relaxation mechanism that is responsible for the dynamic response of a certain nanocomposite structure is still not clear, nor is it clear to what extent that the polymer/clay interaction, intercalation, exfoliation, and dispersion contribute to the observed measurements.

In this report, we discussion the further development of rheological techniques to analyze the clay morphology in a nanocomposite. Previous research [18] has demonstrated the utility of the rheological technique to differentiate (qualify) the degree of exfoliation/dispersion. The objective of this paper is to map out the structure-rheological response of PS nanocomposites with various clay dispersions; and quantify the key parameter that dominates the characteristic rheological response.

2. Experimental

2.1. Materials

The polystyrene used in this study was STYRON™ polystyrene 612 (PS or PS612), produced by the Dow Chemical Company. The two clays used in this study were natural clay, montmorillonite, (MMT) and a synthetic clay, fluorinated synthetic mica (FSM). The organic modifier used here is a 1,2-dimethyl-3-*n*-hexadecyl imidazolium treatment (DMHDI). Additional details on the clays, the organic treatment, sample preparation and the TEM/XRD characterization of those PS nanocomposites are described in a previous paper [19]. The nanocomposite sample names and their previously measured properties are listed in Table 1.

In Table 1, the weight percent of DMHDI treated clay was calculated to give desired percentages of inorganic clay in the final nanocomposite. The different concentration of inorganic clay in the table above represent the

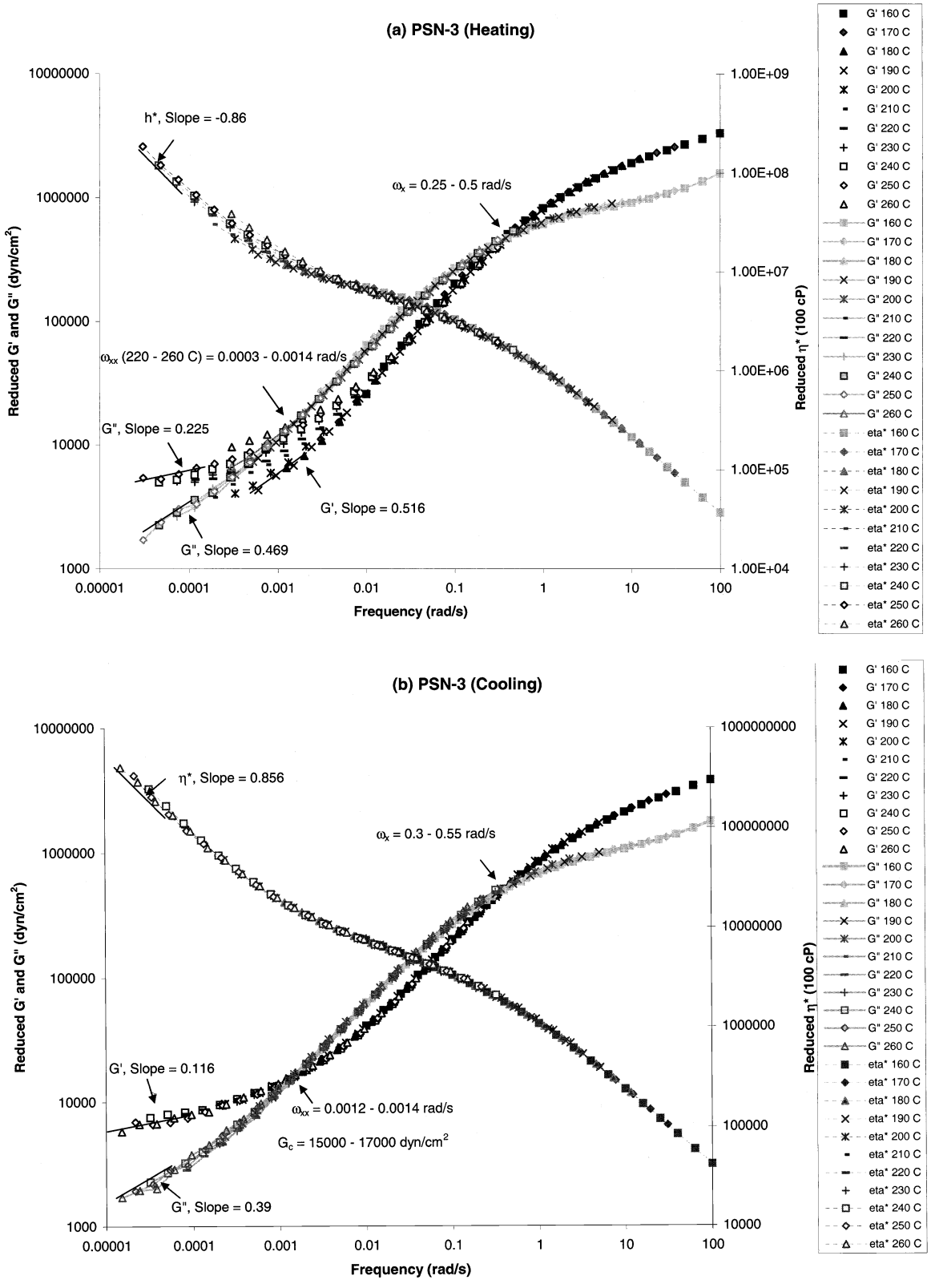

Fig. 4. Reduced frequency dependence of storage modulus, G', loss modulus, G'', and complex viscosity, η^* of PS + 3.63 wt% DMHDI-MMT, no sonication (PSN-3). Master curve (a) was obtained by heating the sample from 160 to 260 °C. Master curve (b) was obtained by annealing the sample at 260 °C and then cooling the sample down from 260 to 160 °C.

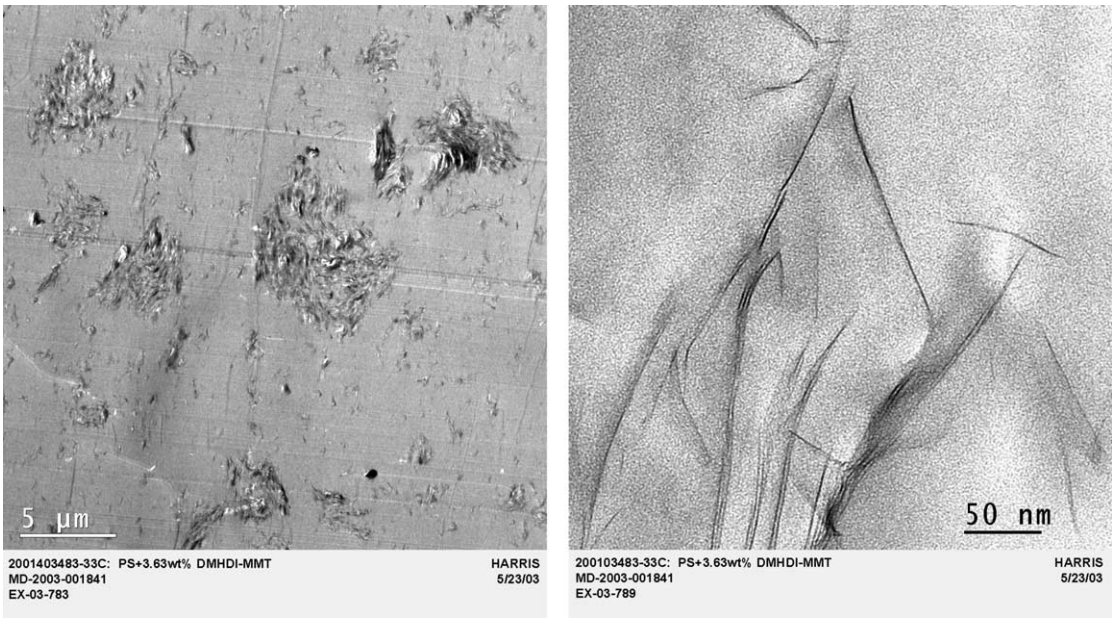

Fig. 5. TEM images of PS + 3.63 wt% DMHDI-MMT (PSN-3), no sonication.

nanocomposites with 1 wt% (PSN-1, PSN-2, PSN-5, PSN-6) and 2.5 wt% (PSN-3, PSN-4, PSN-7, PSN-8) of inorganic clay inside the polymer matrix. All samples in Table 1 were prepared for rheology measurements by compression molding the material into 25 mm diameter disks, and further melting in the vacuum oven. It was then compressed into the desired thickness in the vacuum oven.

2.2. Dynamic shear measurements

Dynamic shear measurements were conducted on ARES rheometer (Advanced Rheometric Expansion System, Rheometric Scientific, RSI Orchestrator software) with a 25 mm diameter parallel plate fixture and a sample thickness of ~2 mm. For dynamic shear measurements, a small-amplitude oscillatory shear,

$$\gamma = \gamma_0 \sin(\omega t) \tag{1}$$

was applied to the sample, and the resultant shear stress was measured as

$$\sigma(t) = \gamma_0[G'(\omega)\sin(\omega t) + G''(\omega)\cos(\omega t)] \tag{2}$$

with $G'(\omega)$ and $G''(\omega)$ being the storage and loss modulus, respectively. A strain sweep was performed to all samples to select a strain amplitude, $<0.6\%$, that is within the linear viscoelastic response of the material. Each frequency scan was performed after 5 min of annealing at the desired temperature. The master curves were generated using the

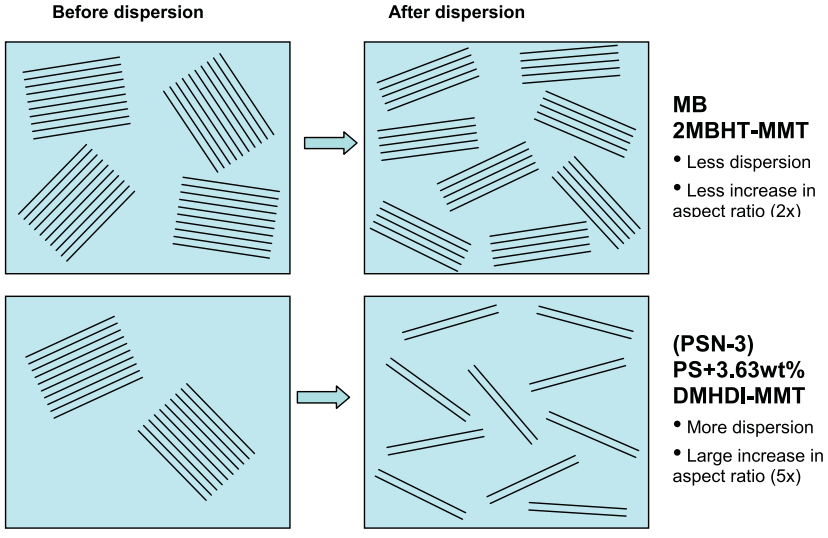

Fig. 6. Schematic representation of speculated clay dispersion mechanism for 2MBHT and DMHDI modified montmorillonite.

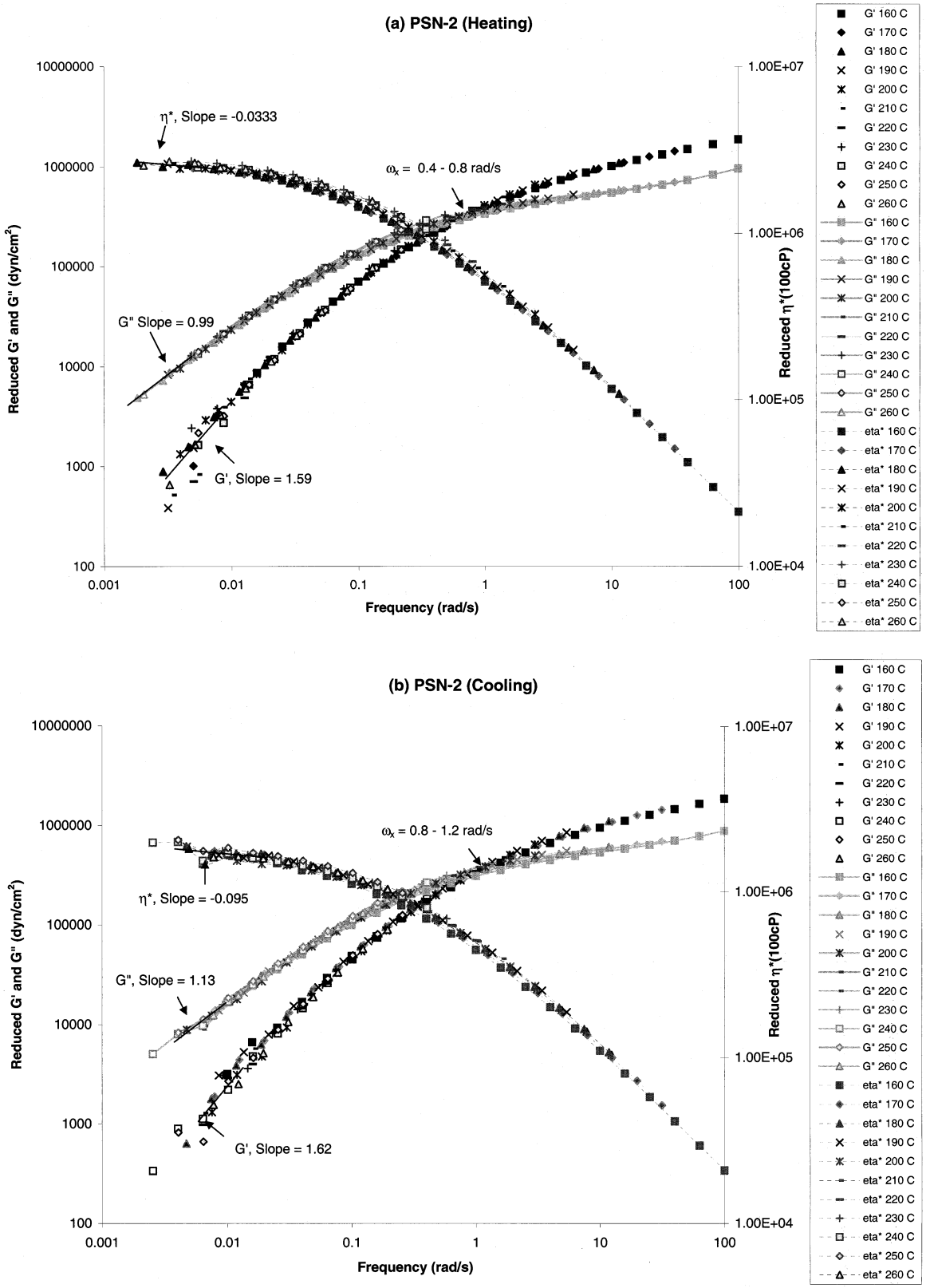

Fig. 7. Reduced frequency dependence of storage modulus, G', loss modulus, G'', and complex viscosity, η^* of PSN-2 (PS + 1.48 wt% DMHDI-FSM, no sonication). Master curve (a) was obtained by heating the sample from 160 to 260 °C. Master curve (b) was obtained by annealing the sample at 260 °C and then cooling the sample down from 260 to 160 °C.

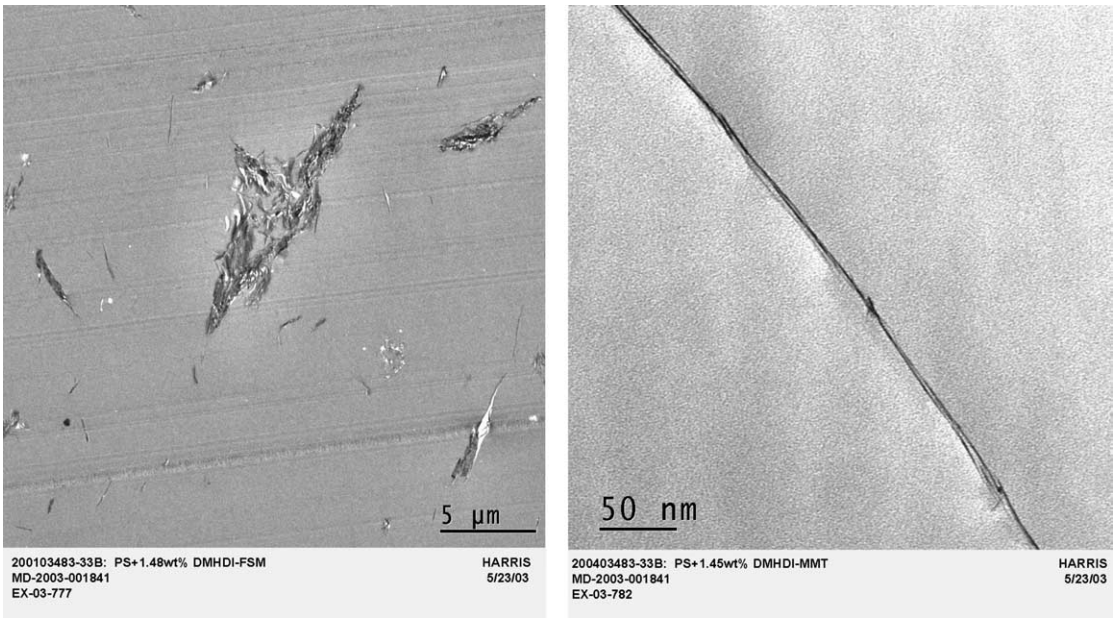

Fig. 8. TEM images of PSN-2 (PS + 1.48 wt% DMHDI-FSM, no sonication).

principle of time–temperature superposition and shifted to a common reference temperature (T_{ref}) of 160 °C.

2.3. Thermal analysis

Differential scanning calorimetry of the samples were done using DSC Q-1000 (TA instruments). The samples were heated from 30 to 260 °C at 5 °C per minute, holding the temperature at 260 °C for 4 min, and cooling it back down to 30 °C at 5 °C per minute. This sequence was repeated four more times. Analysis for the glass transition temperature T_g was done for each cycle.

3. Results and discussion

3.1. Nanocomposite morphology

In a previous paper [19], we describe the synthesis of PS clay nanocomposites prepared by solvent blending methods, with and without sonication. These samples were extensively characterized by XRD and TEM, verifying degrees of polymer intercalation, as well as clay dispersion. These well-characterized materials were synthesized solely for the purpose of providing known intercalated/exfoliated samples for polymer melt rheology analysis. The non-sonicated samples, while having significant amounts of polymer intercalation, were poorly dispersed nanocomposites by TEM. Only when sonication was applied did the clay exfoliate in the PS matrix. The clay type did affect the degree of clay exfoliation, with the montmorillonite samples (DMHDI-MMT) exfoliating completely with sonication, and the fluorinated synthetic mica (DMHDI-FSM) dispersing well, but not fully exfoliating.

3.2. Dynamic shear measurements

Usually, a dynamic spectrum can be used to understand the structure and properties of polymers. To access a broad frequency range of the material, a principle, so called time–temperature superposition (TTS) principle is often used. It states that time and temperature have equivalent effects on the rheological properties of linearly viscoelastic materials. Mathematically this principle can be expressed as

$$G'(\omega, T_r) = \frac{\rho(T_r)T_r}{\rho(T)T} G'(a_\tau \omega, T) \tag{3}$$

$$G''(\omega, T_r) = \frac{\rho(T_r)T_r}{\rho(T)T} G''(a_\tau \omega, T) \tag{4}$$

where the subscript r refers to conditions at a reference temperature, a_τ is the ratio of relaxation times at two temperatures, i.e. $\lambda_k(T)/\lambda_k(T_r)$, and $\rho(T)$ is the density of polymers at temperature T [20,21]. However, this principle is only valid when all of the relaxation times λ_k in Maxwell equation have the same temperature dependence $a_\tau(T)$. Some polymer systems, including polymer nanocomposites, will not simply follow this principle due to the rheological complexity that results from ordered microstructures. The detailed discussion and examples of this complexity were shown in the previous paper [18]. To further understand how these dynamic spectrum correlate and compare to nanocomposite dispersion, it was essential to use a well-characterized sample, which had undergone TEM and XRD analysis. To assist in the explanation of how the rheology

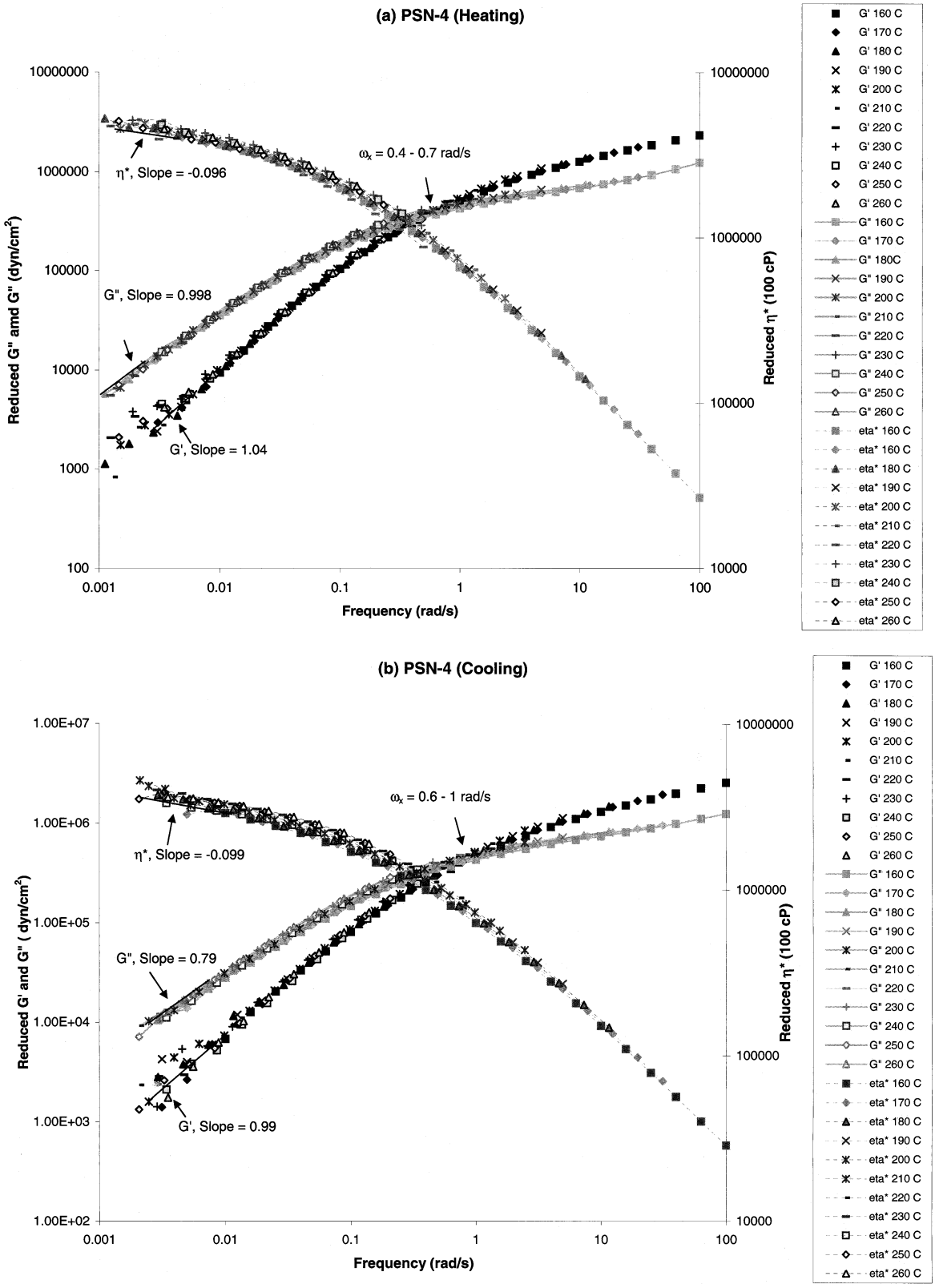

Fig. 9. Reduced frequency dependence of storage modulus, G', loss modulus, G'', and complex viscosity, η^* of PSN-4 (PS + 3.72 wt% DMHDI-FSM, no sonication). Master curve (a) was obtained by heating the sample from 160 to 260 °C. Master curve (b) was obtained by annealing the sample at 260 °C and then cooling the sample down from 260 to 160 °C.

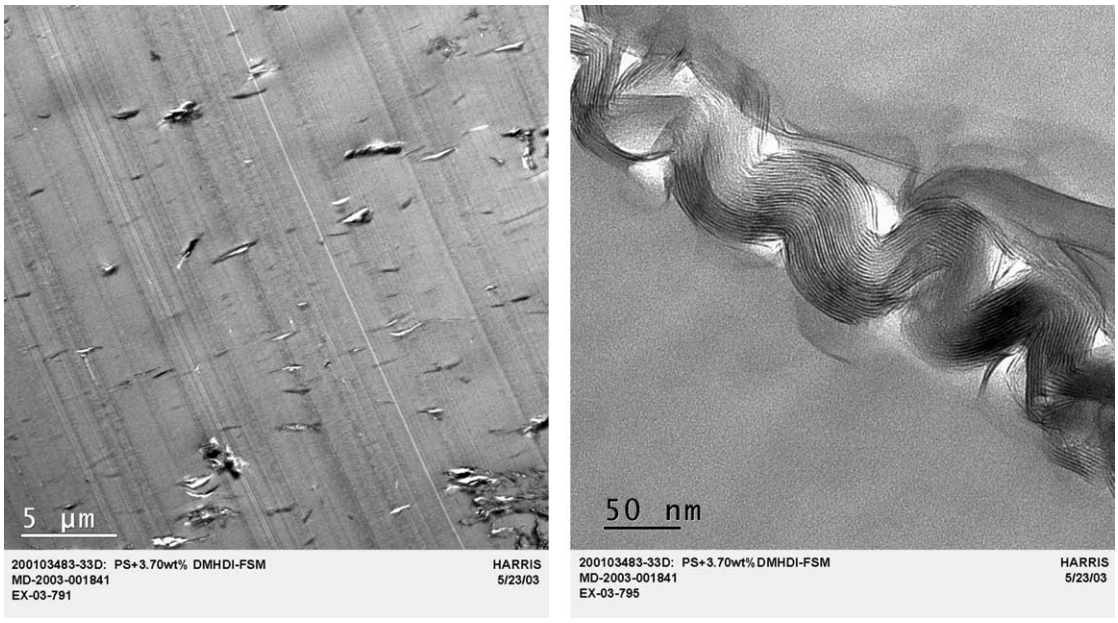

Fig. 10. TEM images of PSN-4 (PS + 3.72 wt% DMHDI-FSM, no sonication).

data relates to the nanocomposite dispersion, TEM images form the previous work [19] are shown below each corresponding spectra.

The dynamic mechanical spectrum of pure PS, i.e. PS612, and all samples listed in Table 1 were investigated using isothermal frequency scans, as shown in Figs. 1, 2, 4, 7, 9, 11, 13, 15, and 17. In Figs. 2, 4, 7, 9, 11, 13, and 15, graph (a) shows the TTS data generated by heating up the sample while graph (b) was generated by annealing at 260 °C and cooling down the sample. The isothermal frequency scans were then temperature and density corrected according to Eqs. (3) and (4) and time–temperature superpositioned based on a common reference temperature (T_{ref} = 160 °C). The spectrum of pure PS is shown in Fig. 1. As expected, it shows a longest relaxation time $\tau \sim (1/\omega_x) \sim (1.11–1.67)$, where $\omega_x \sim 0.6–0.9$ rad/s is the frequency that G' and G'' crossover. Fig. 1 also shows a typical polymer terminal relaxation behavior ($G' \sim \omega^{1.5} \sim \omega^2$, $G'' \sim \omega^{0.98} \sim \omega$). In addition, the master curve obtained by heating up from 160 to 260 °C is similar to the master curve obtained by cooling down the sample from 260 to 160 °C.

The spectra of the PSN-1 nanocomposite were similarly generated and are shown in Fig. 2(a) and (b). Note that the fluctuation of the data at low frequencies was probably caused by small torque signal that was close to instrument resolution limit. Again, time–temperature superposition works well in this case. However, the overall patterns of the spectra or relaxation behavior of the material has changed. Fig. 2(b) shows that both G' and G'' approach a slope of 1, i.e. ($G' \sim \omega$, $G'' \sim \omega$) after being annealed at 260 °C. The crossover frequencies associated with the longest relaxation time for this particular nanocomposite are similar to that of pure PS.

As the concentration of the inorganic clay content increases from 1 wt% (PSN-1) to 2.5 wt% (PSN-3), the dynamic mechanical spectrum changes again as shown in Fig. 4. Time–temperature superposition failed when constructing the master curves from the scans obtained by heating up the sample (Fig. 4(a)), but still valid when the sample was annealed for 5 min at 260 °C and cooled back down to 160 °C (Fig. 4(b)). The heating scans, however, can be time–temperature superpositioned using high frequency branches. This is consistent with the previously reported results [18].

Fig. 4(b) shows that the frequency dependence of G' and G'' of the PSN-3 nanocomposite exhibits two crossover frequencies where G' and G'' cross, ω_x = 0.3–0.55 rad/s and

Table 2
The glass transition temperature for polystyrene nanocomposites

Sample name	Description	Cycle (°C)	T_g (°C)
PSN-1	PS + 1.45 wt% DMHDI-MMT solvent-stirring, no sonication	30–260	104.3
PSN-2	PS + 1.48 wt% DMHDI-FSM solvent-stirring, no sonication	30–260	103.8
PSN-3	PS + 3.63 wt% DMHDI-MMT solvent-stirring, no sonication	30–260	103.6
PSN-4	PS + 3.72 wt% DMHDI-FSM solvent-stirring, no sonication	30–260	104.5
PSN-5	PS + 1.45 wt% DMHDI-MMT solvent + sonication	30–260	104.5
PSN-6	PS + 1.48 wt% DMHDI-FSM solvent + sonication	30–260	104.3
PSN-7	PS + 3.63 wt% DMHDI-MMT solvent + sonication	30–260	103.6
PSN-8	PS + 3.72 wt% DMHDI-FSM solvent + sonication	30–260	103.6
Styron 612	PS control	30–260	103.2

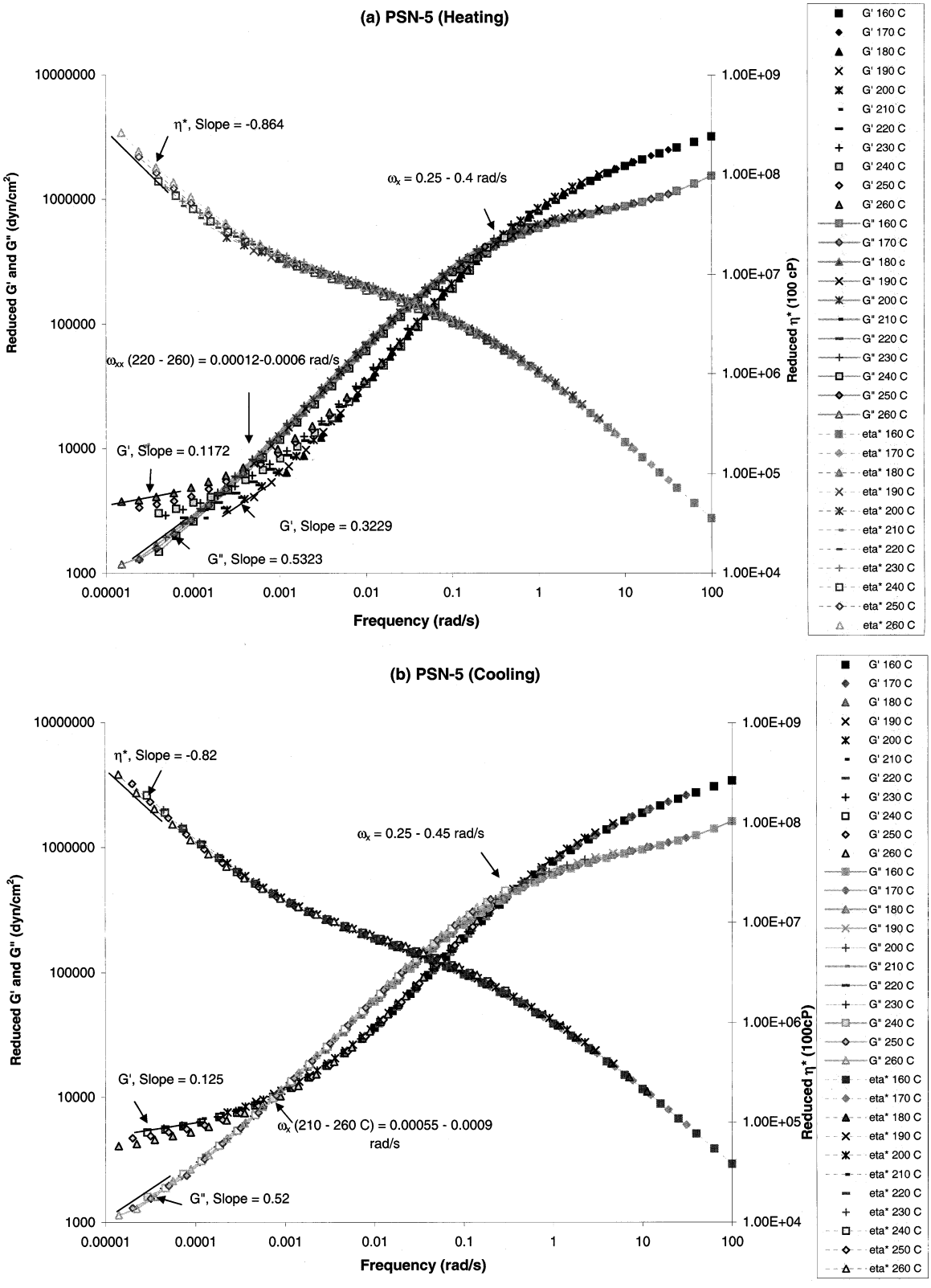

Fig. 11. Reduced frequency dependence of storage modulus, G', loss modulus, G'', and complex viscosity, η^* of PSN-5 (PS + 1.45 wt% DMHDI-MMT, with sonication). Master curve (a) was obtained by heating the sample from 160 to 260 °C. Master curve (b) was obtained by annealing the sample at 260 °C and then cooling the sample down from 260 to 160 °C.

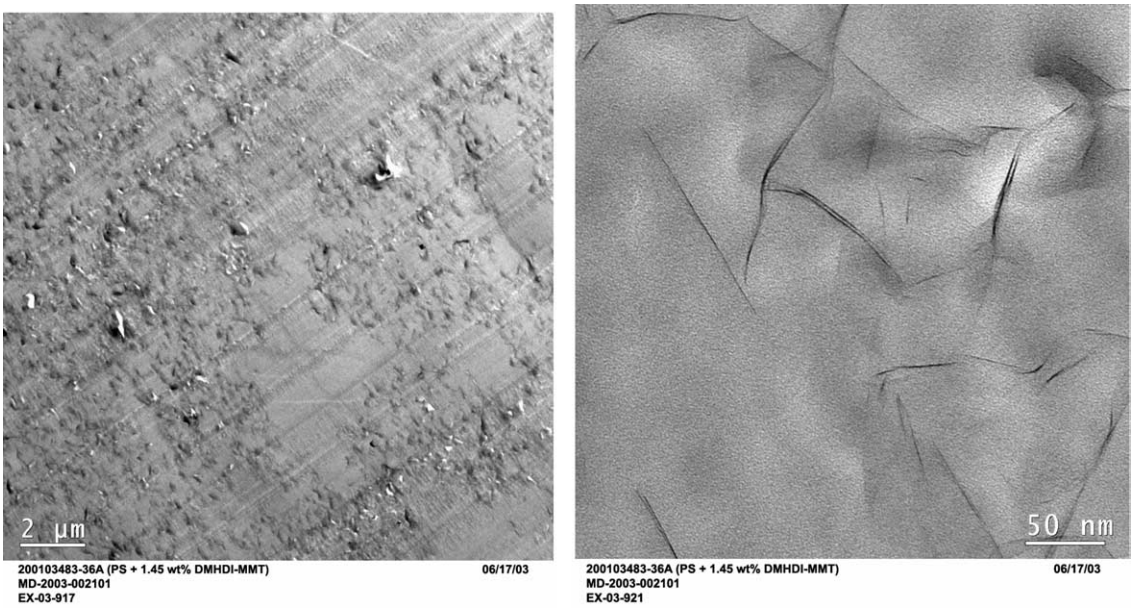

Fig. 12. TEM images of PSN-5 (PS + 1.45 wt% DMHDI-MMT, with sonication).

ω_{xx} = 0.00012–0.0014, and correspondingly three distinct regions. At high frequencies (region I), $\omega > \omega_x$, the response of polymer chains dominate, a rubbery elastic plateau can be observed. At intermediate frequencies (region II), $\omega_{xx} < \omega < \omega_x$, the interplay of the clays with polymer chains results a more dissipative but non-terminal like response. At low frequencies (region III), $\omega < \omega_{xx}$, G' becomes greater than G'' and also becomes independent of frequency, which is characteristic of a solid like response. At this low frequency region, viscosity shows a slight shear-thinning behavior with a shear thinning exponent $n = -0.86$, where η^* can be modeled by the following equation:

$$\eta* = A\omega^n \tag{5}$$

Since, the *d*-spacing and thus the amount of intercalation is similar between the PSN-1 and PSN-3 samples, the different dynamic spectrum pattern must come from the different amount of clay particles per unit volume presented in the sample. This assumes that the aspect ratios of the clays in these two samples are roughly the same, as evident by comparing Figs. 3–5. Further, the aspect ratio for the DMHDI-MMT samples can be assumed to be the same since the same organoclay (DMHDI-MMT) was used.

The spectrum of PSN-3 was also very similar to the spectrum of a different PS nanocomposite using a MMT clay [sample MB in previous paper] [18]. Sample MB was made by melt blending PS and dimethyl, benzyl, hydrogenatedtallow, quarternary ammonium (2MBHT) modified MMT, and had a concentration of 5.2 wt% of inorganic MMT. In contrast to the spectrum of PSN-3 with 2.5 wt% of inorganic content, sample MB which has 5.2 wt% inorganic content showed a similar spectrum. The terminal modulus of G' and η^* of PSN-3 (5.8×10^3 dyn/cm^2 and 4.0×10^8 P, respectively) were higher than the G', η^* (2.17×10^3 dyn/cm^2 and 6.4×10^7 P, respectively) obtained from sample MB. The high frequency modulus G' for the PSN-3 was around 3.8×10^6 dyn/cm^2, which was also higher than that of sample MB (about 1.8×10^6 dyn/cm^2). As indicated earlier, when comparing PSN-1 and PSN-3, it seems that the number density of clay particles dominates the rheological response of the nanocomposites. The fact that PSN-3 shows similar patterns to sample MB indicates that the number of particles per unit volume for this sample is about the same, or even greater, than that of sample MB in the previous report. This suggests that sample PSN-3 with DMHDI-modified MMT is better dispersed than sample MB, which has 2MBHT-modified MMT and processed by melt blending. Even though MB has a higher concentration of clay initially, the final number density of its clay particles is less or equivalent to that of PSN-3. The relative degree of dispersion between these two samples is schematically represented in Fig. 6.

Fig. 7(a) and (b) shows the dynamic mechanical spectra for PSN-2, which basically are very similar to the response of pure PS. Again, the time–temperature superposition works well in both heating and cooling curves. This sample has the same amount of inorganic clay as PSN-1 ($\sim$1 wt%), but the clay is FSM instead of MMT. MMT samples showed better dispersion than the FSM samples [19] which explains why the rheological response of PSN-2 is closer to the pure PS matrix polymer than that of PSN-1 which has 1 wt% of MMT.

Fig. 9(a) and (b) shows the dynamic mechanical spectra of PSN-4 containing 2.5 wt% inorganic content. It follows a similar pattern as PSN-2, which has 1 wt% inorganic content. But PSN-4 has a terminal response of $G' \sim \omega$, $G'' \sim \omega$, which is similar to PSN-1. As the concentration of FSM in the polymer matrix is increased from 1 wt%

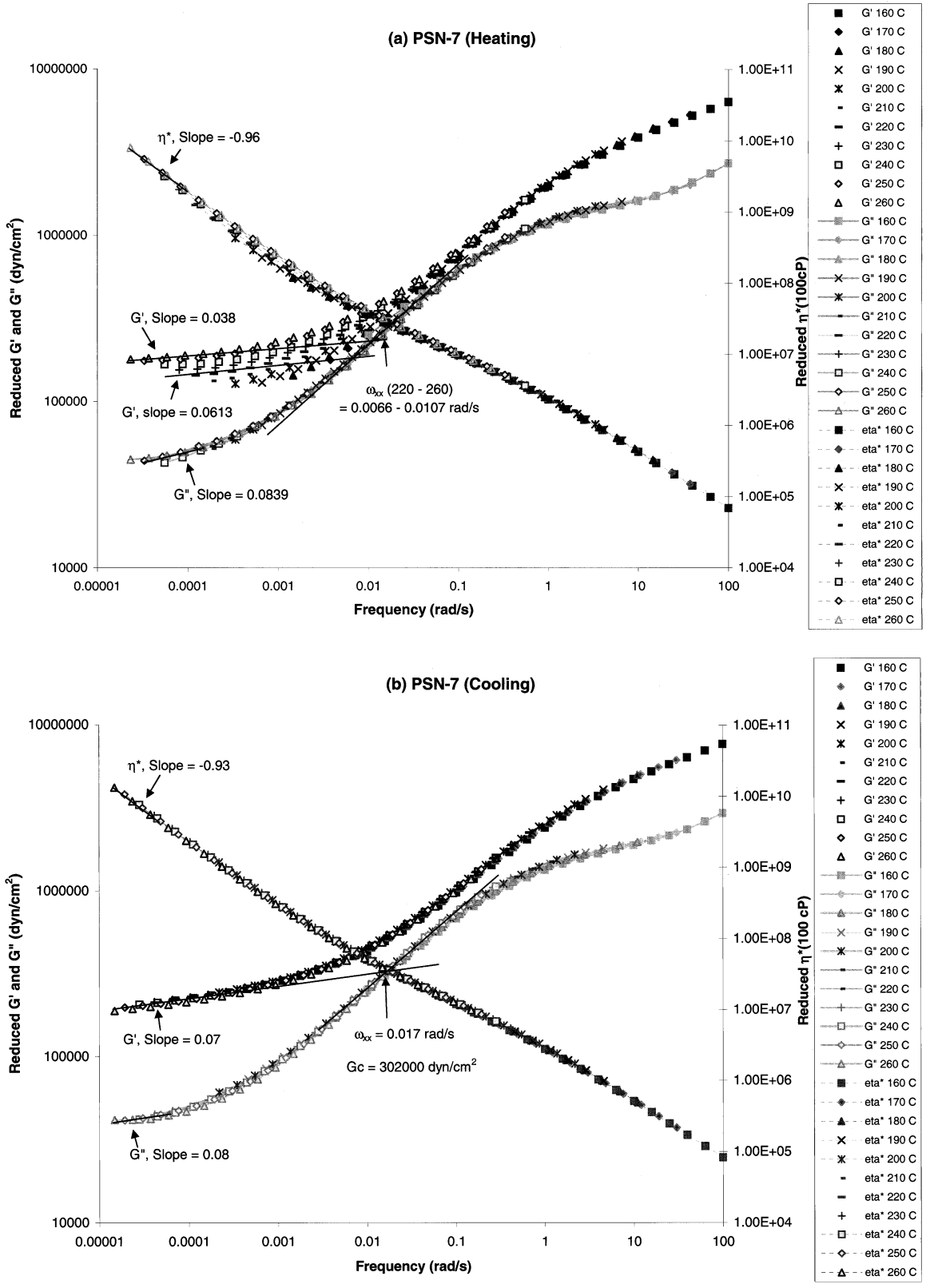

Fig. 13. Reduced frequency dependence of storage modulus, G', loss modulus, G'', and complex viscosity, η^* of PSN-7 (PS + 3.63 wt% DMHDI-MMT, with sonication). Master curve (a) was obtained by heating the sample from 160 to 260 °C. Master curve (b) was obtained by annealing the sample at 260 °C and then cooling the sample down from 260 to 160 °C.

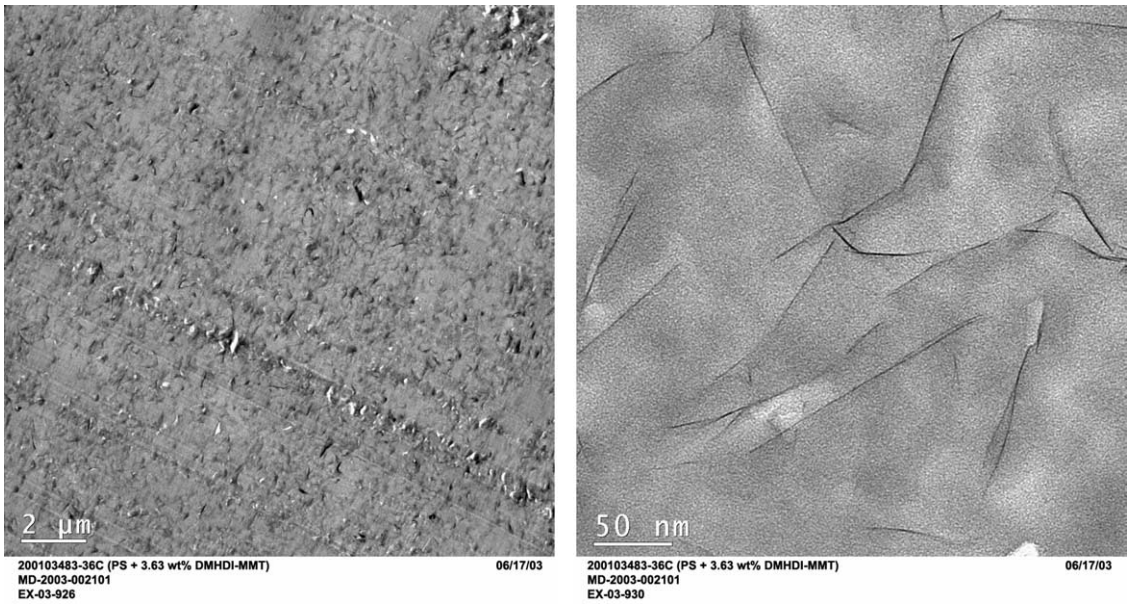

Fig. 14. TEM images of PSN-7 (PS + 3.63 wt% DMHDI-MMT, with sonication).

(PSN-2) to 2.5 wt% (PSN-4), and thus the particle number density is increased from PSN-2 (Fig. 8) to PSN-4 (Figs. 9 and 10), the dynamic mechanical spectrum changes in the terminal relaxation regime. Both G' and G' of PSN-4 approach a slope of 1 in the low frequency regime ($G' \sim \omega^{0.79} \sim \omega$, $G'' \sim \omega^{0.99} \sim \omega$, Fig. 9(b)). In contrast, PSN-2 spectrum which contains 1 wt% of FSM shows a typical polymer terminal relaxation behavior ($G' \sim \omega^2$, $G'' \sim \omega$) in Fig. 7(b).

When the PS + DMHDI treated clay samples were mixed with solvent blending and sonication, the dynamic mechanical spectra for all samples changed. Fig. 11(a) and (b) shows the dynamic mechanical spectra of sample PSN-5 nanocomposites. The frequency dependence of G' and G'' shows two crossover frequencies, $\omega_x = 0.25$–0.45 rad/s and $\omega_{xx} = 0.00055$–0.0009. The composition of sample PSN-5 is the same with PSN-1 except that PSN-5 is mixed by high energy sonication. The TEM image (Fig. 12) [19] for sample PSN-5 showed that sonication helped to reach better exfoliation and more dispersed particles than that of the PSN-1 sample. This explains why the dynamic mechanical spectrum for PSN-5 (Fig. 11) is rather similar to PSN-3 (Fig. 4) than that of PSN-1 (Fig. 2). This further confirms our hypothesis that the number of particles per unit volume inside the polymer matrix is a key factor that determines the rheological response of nanocomposite materials.

As the amount of inorganic clay increased from 1 wt% (PSN-5) to 2.5 wt% (PSN-7), the number density of particles increased from that of PSN-5 (Fig. 12) to that of PSN-7 (Fig. 14), the dynamic mechanical spectrum changed as shown in Fig. 8(a) and (b), which are obtained from sample PSN-7. Again, time temperature superposition was not possible when constructing the master curves from the scans obtained by heating up the sample (Fig. 13(a)), but still valid when the sample was annealed for 5 min at 260 °C and cooled back down to 160 °C (Fig. 13(b)). The spectrum of sample PSN-7 has a considerably higher modulus than all other samples tested. The modulus G' lies well above G'' in all frequency range. The complex viscosity η^* showed a shear thinning component $n = -0.96$ and a pseudo-crossover frequency $\omega_{xx} = 0.0066$–0.0107 rad/s (obtained by extrapolation from low frequency G' and G'' as shown in Fig. 13). This solid-like response indicates a percolated organization of the platelets in a network-like superstructure [18].

Since, the d-spacing and thus the amount of intercalation is similar between PSN-5 and PSN-7 (Table 1), the different dynamic spectrum pattern again comes from the different number density of particles present in the sample. This observation supports the hypothesis that the key factor which determines the rheological response of nanocomposite is the number density, or number of clay plates per clay particle.

Fig. 13(b) is also very similar to the master curve obtained from sample SB in the previously reported work [18]. However, the spectrum of PSN-7 was reached by using only 2.5 wt% of inorganic content. In the previous report, similar spectrum of sample SB was obtained based on the sample with 5.2 wt% of inorganic content. In addition, the terminal modulus of G' and η^* of PSN-7 (1.9×10^5 dyn/cm^2 and 1.32×10^{10} P, respectively) are similar the G', η^* (2.28×10^5 dyn/cm^2 and 3.1×10^{10} P, respectively) that obtained from sample SB[1]. The high frequency modulus G' for PSN-7 is around 7.72×10^6 dyn/cm^2; this is higher than that of sample SB, which is about 2.93×10^6 dyn/cm^2.

As indicated earlier, when comparing PSN-1 and PSN-3, it seems that the number of clay particles per unit volume dominates the rheological response of the nanocomposites.

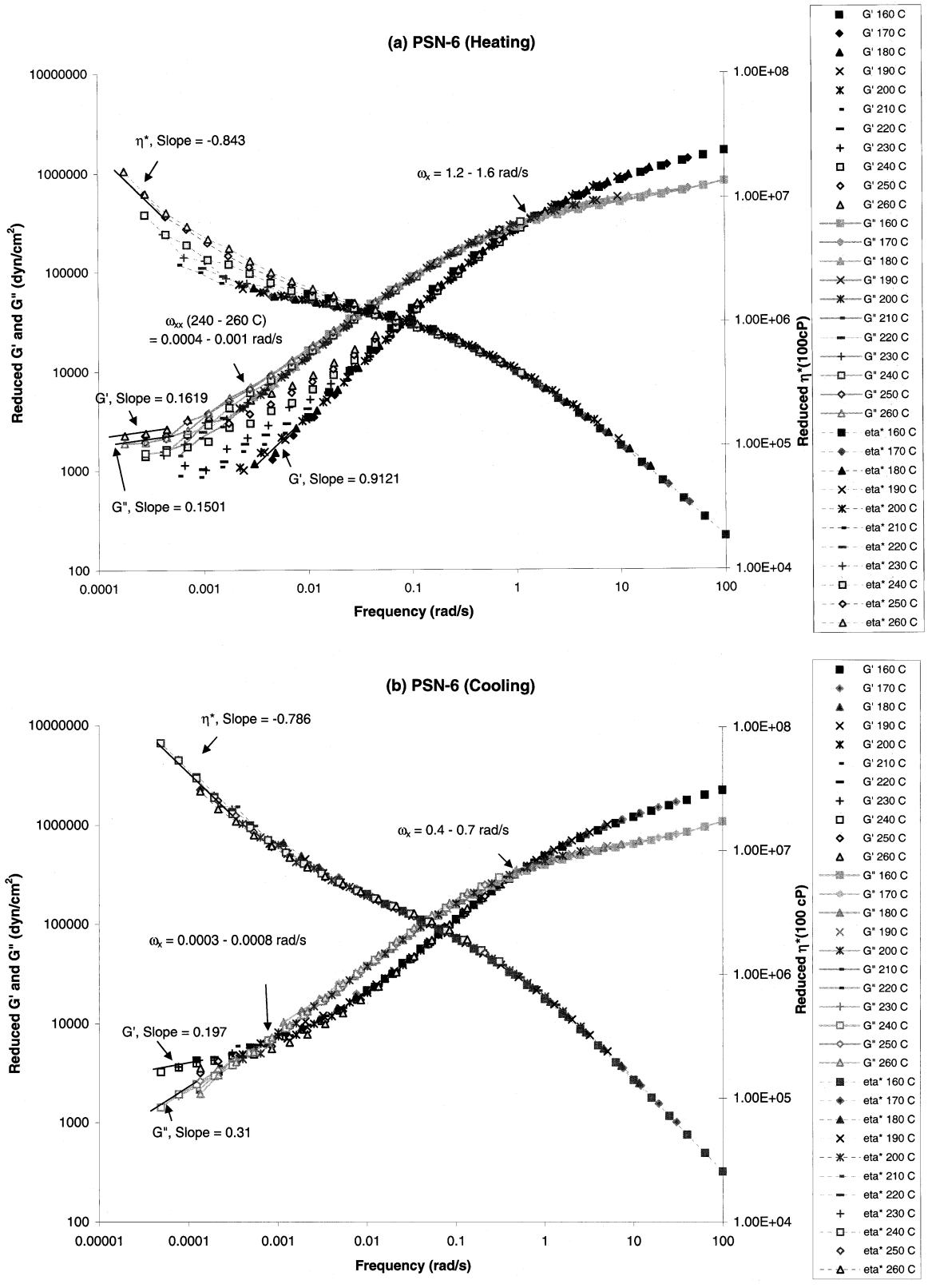

Fig. 15. Reduced frequency dependence of storage modulus, G', loss modulus, G'', and complex viscosity, η^* of PSN-6 (PS + 1.48 wt% DMHDI-FSM, with sonication). Master curve (a) was obtained by heating the sample from 160 to 260 °C. Master curve (b) was obtained by annealing the sample at 260 °C and then cooling the sample down from 260 to 160 °C.

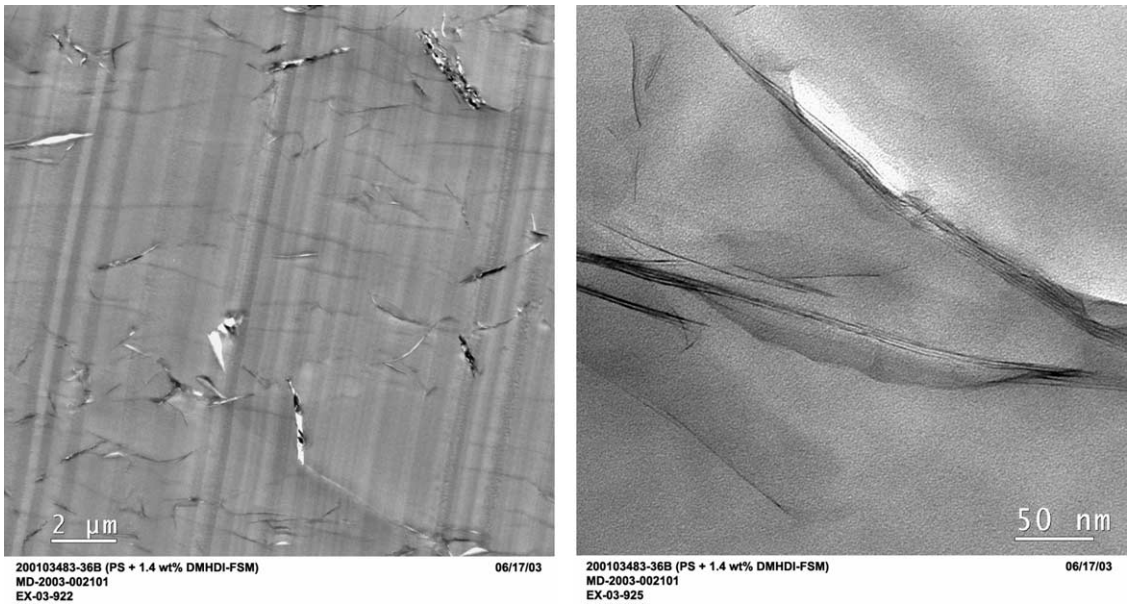

Fig. 16. TEM images of PSN-6 (PS + 1.48 wt% DMHDI-FSM, with sonication).

The fact that PSN-7 shows similar pattern to sample SB indicates that the particle number density of PSN-7 is about the same to the sample SB in the previous report. These data show that the organic modifier of DMHDI used in PSN-7 combined with high energy sonication is more efficient in dispersing the clay than the process of making sample SB using 2MBHT modified clay. This is consistent with the comparison of PSN-1 and PSN-3 we presented earlier.

Sample PSN-7 contains the same composition of MMT clay as sample PSN-3 except that sonication is used. As shown earlier, among all the non-sonicated samples, the dynamic mechanical spectrum of PSN-3 (Fig. 4) is the only one that shows double crossover frequencies, probably due to better dispersion of clay particles leading to a particle number density close to percolation threshold. The use of sonication during solvent blending synthesis affects the dynamic mechanical spectra of these samples greatly. Sample PSN-7 (Fig. 13(b)) shows a pattern that represents a percolated network structure which means the particle number density is higher than the percolation threshold. Therefore, sonication helps sample PSN-7 to approach a better exfoliation (Fig. 14).

The spectra obtained from PSN-6 are shown in Fig. 15(a) and (b). The spectra of PSN-6 show a rheological response that have a pattern that is similar to the spectra obtained from sample PSN-3, which indicates a particle number density close to percolation threshold. When comparing the spectra of PSN-6 with that of PSN-4, the modulus and viscosity of PSN-6 in the high frequency regime ($G' \sim 2.31\times10^6$ dyn/cm^2, $\eta^* \sim 2.57\times10^4$ P) are similar to that of PSN-4 ($G' \sim 2.58\times10^6$ dyn/cm^2, $\eta^* \sim 2.87\times10^4$ P). In addition, the pattern of PSN-4 with a terminal response of $G' \sim \omega$, $G'' \sim \omega$ also indicates a dominant polymer behavior with clay interacting with polymer chains. Based on previous analysis, the particle number density of sample PSN-6 is about equivalent to sample PSN-4 even though PSN-6 has lower clay concentration than PSN-4 (an analogous situation is schematically presented in Fig. 6). This difference can be caused by different charge distribution between FSM and MMT clay [22]. Higher cation exchange capacity may result in more ionic charge between each clay plate, which makes it more difficult to exfoliate FSM clays (Fig. 16).

Fig. 17(a) and (b) shows the spectra for sample PSN-8, which follow a similar pattern of sample PSN-6. However, the terminal modulus of PSN-8 ($G' = 1.25\times10^4$ dyn/cm^2 and $\eta^* = 4.63\times10^8$ P) is higher than that of PSN-6 ($G' = 3.23\times10^3$ dyn/cm^2 and $\eta^* = 7.24\times10^7$ P). Furthermore, the distance between the two crossover frequencies for PSN-8 ($\omega_x = 0.25$–0.5 rad/s and $\omega_{xx} = 0.0007$–0.0014 rad/s) is less than that of PSN-6 ($\omega_x = 0.4$–0.7 rad/s and $\omega_{xx} = 0.0003$–0.0008 rad/s). This translates to a lower characteristic time difference, $\tau_{xx} - \tau_x = (2\pi/\omega_{xx}) - (2\pi/\omega_x)$, for PSN-8 ($\tau_{xx} - \tau_x = 4715.2$ s in average), than that for PSN-6 ($\tau_{xx} - \tau_x = 8538.5$ s in average). Note that in contrast to unsonicated samples PSN-2 and PSN-4, both PSN-6 and PSN-8 have two crossover frequencies, which is due to a better dispersion of clay particles by using sonication as explained earlier. Previous work [19] indicated that PSN-8 has a higher number density than PSN-6 (Table 1). The characteristic of their dynamic mechanical response indicates that PSN-8 is the sample that has the highest particle number density among all FSM-based nanocomposites investigated in this paper.

By comparing PSN-7 and PSN-8 which both have 2.5 wt% inorganic clay, we can see that shear thinning exponent of MMT-based nanocomposite (PSN-7) is higher than that of FSM-based nanocomposites (PSN-8). High

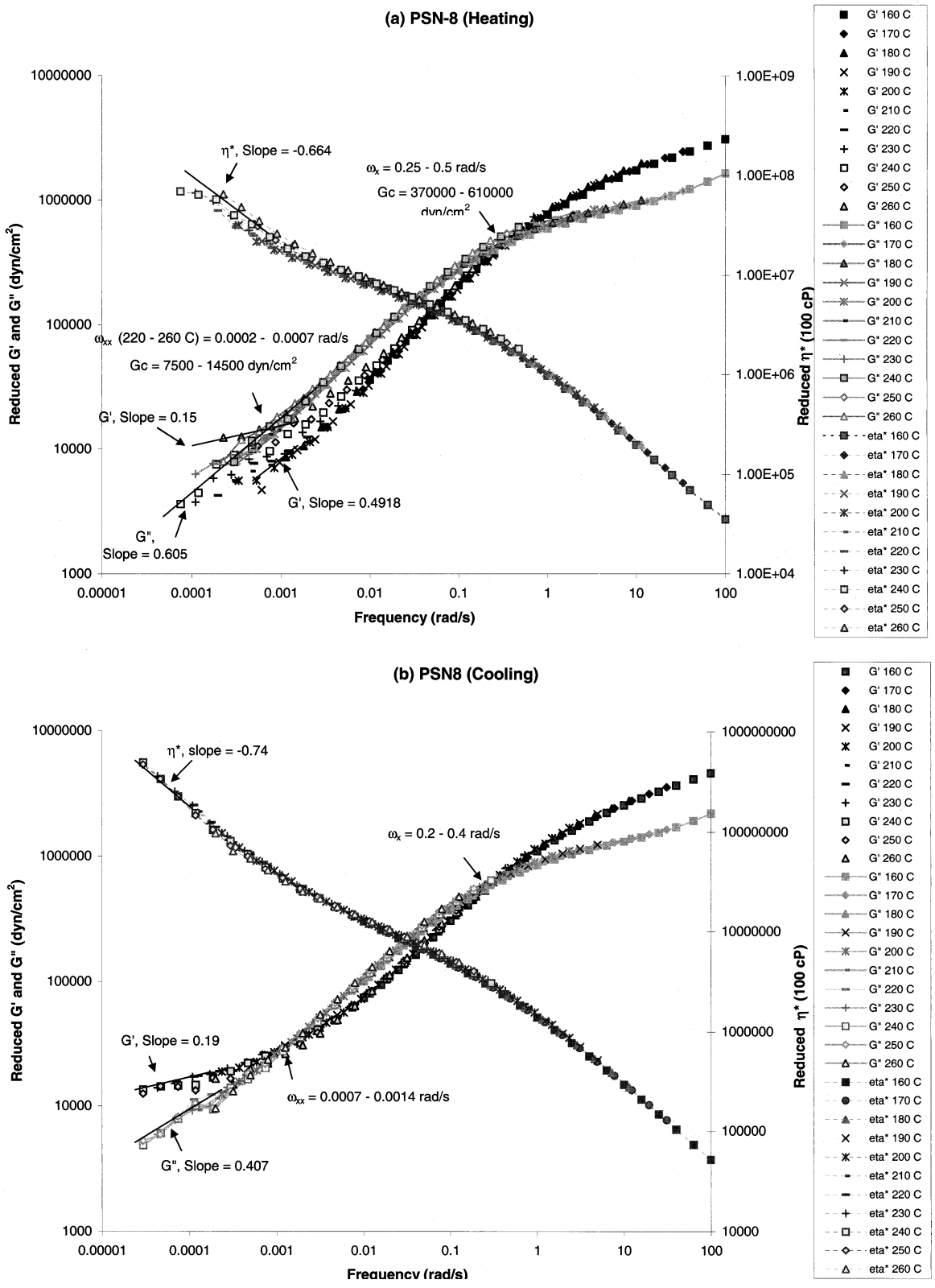

Fig. 17. Reduced frequency dependence of storage modulus, G', loss modulus, G'', and complex viscosity, η^* of PSN-8 (PS + 3.72 wt% DMHDI-FSM, with sonication). Master curve (a) was obtained by heating the sample from 160 to 260 °C. Master curve (b) was obtained by annealing the sample at 260 °C and then cooling the sample down from 260 to 160 °C.

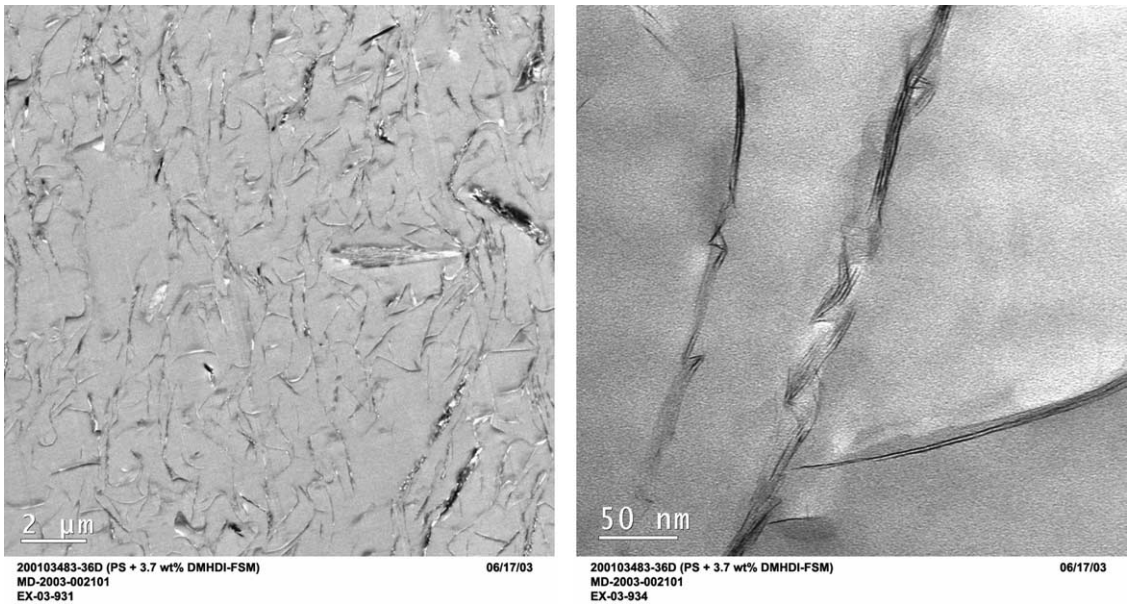

Fig. 18. TEM images of PSN-8 (PS + 3.72 wt% DMHDI-FSM, with sonication).

shear thinning exponent of PSN-7 indicates the degree of the change of clay orientation under flow in PSN-7 is greater than that of PSN-8. This may be caused by a convolution effect of less clay layers per particle and higher particle number density of PSN-7 than that of PSN-8 (Fig. 18).

In summary, a schematic rheological response to the different level of clay dispersion is shown in Fig. 19, based on the experimental data presented in this report. Pure polystyrene and a PS matrix with a low level of clay particles gives a typical terminal relaxation behavior for polymer ($G' \sim \omega^2$, $G'' \sim \omega$). Incorporation of more clay particles into the polymer would result in a change of the spectrum in the terminal relaxation regime (both G', $G'' \sim \omega$). As the level of dispersion increases, G' and G'' spectrum will show more solid like behavior, especially at low frequencies ($G' > G''$, $G'' \sim \omega^0$). Further increase in the clay dispersion would produce a response where G' is greater than G'' across all frequencies, indicating a percolated network structure.

3.3. Thermal analysis result

Table 2 shows DSC data for all the nanocomposite samples investigated in this paper. The glass transition

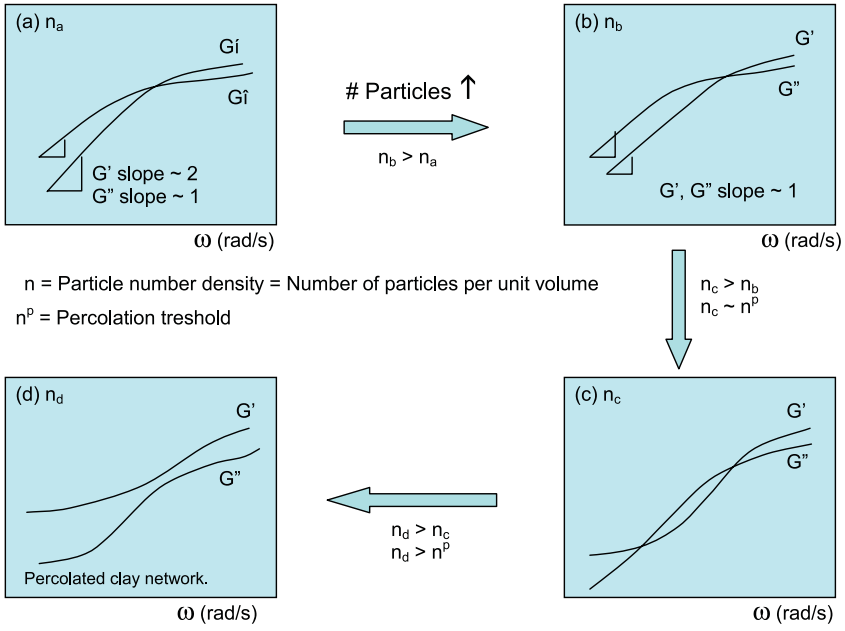

Fig. 19. The schematic representation of the speculated rheological response to the increase in the number of particles per unit volume.

temperatures obtained from multiple cycles were very similar. The glass transition temperatures for all samples are about the same regardless of composition or clay dispersion. Therefore, thermal analysis on glass transition temperature was not very sensitive to the level of clay dispersion inside the polymer matrix.

4. Conclusions

In this work, we mapped out a series of rheological responses of polystyrene nanocomposite to various clay types, clay concentrations, and degrees of clay dispersion. The level of dispersion, characterized by XRD and TEM, was correlated with a characteristic rheological response. The PS nanocomposites investigated here demonstrate a change of pattern, as a function of the degree of exfoliation, from typical polymer response to a terminal response of $[G' \sim \omega,\ G'' \sim \omega]$, then to a pattern with double crossover frequencies, and finally to a solid-like response with $G' > G''$ in all frequency ranges. We showed that the number of particles per unit volume is a key factor determining the characteristic response for clay-nanocomposites. Measurement of the key characteristic parameters such as shear thinning exponent, elastic plateau at low frequencies and crossover frequencies along with the overall pattern of $G'(\omega)$ and $G''(\omega)$ provides a valuable 'fingerprint' that aids in the characterization of global exfoliation, and in determining the percolation threshold. As a continued investigation from previous study, the rheological response of PS nanocomposites made from DMHDI modified clays combined with high-energy sonication was compared with that of nanocomposites made by 2MBHT modified clay. We found that PS nanocomposites made by DMHDI-modified clay with high-energy sonication is better dispersed than the composites made previously using 2MBHT-modified clay (MB and SB samples previously reported [18]). Without the TEM and XRD characterization first of these materials, however, it would have been difficult to correlate the melt rheology data to the level of clay dispersion. We also showed that the glass transition temperatures were not very sensitive to the degree of dispersion.

As discussed earlier, the broad objective of this research is to develop a rheological technique to analyze the clay morphology in a polymer–clay nanocomposite, especially the relationship between the degree of dispersion and the characteristic rheological response. Even though the quantitative correlation between hybrid structure and rheological properties are still not defined at this moment, this report further demonstrates the utility of the rheological technique to map out the relationship between the degree of dispersion and the characteristic rheological response. More experimental and theoretical work are needed to quantify the structure-rheological property relationship of polymer nanocomposites, to demonstrate the utility of this technique in understanding the influence of material options and processing conditions for improving nanocomposite exfoliation/dispersion.

Acknowledgements

The authors would like to thank Valeriy Ginzburg and Juan Garces for extensive discussions on nanocomposite theories and experimental results, Jane Wardhana for patiently doing endless rheological experiments, Kenn Bouchard and Bryan Roth for their extensive help in rheology testing, and Rich Fibiger, Hoang Pham, Forest Busby for encouragement and support.

References

[1] CMSinfo, http://www.biz-lib.com/ZBUP234.html; 2004.
[2] AzoNanotechnology, http://www.azonano.com/details.asp?ArticleID=1017; 2004.
[3] Dennis HR, et al. Effect of melt processing conditions on the extent of exfoliation in organoclay-based nanocomposites. Polymer 2001;42:9513–22.
[4] Morgan AB, Gilman JW. Characterization of polymer-layered silicate (clay) nanocomposites by transmission electron microscopy and X-ray diffraction: a comparative study. J Appl Polym Sci 2003;87:1329–38.
[5] Alexandre M, Dubois P. Polymer-layered silicate nanocomposites: preparation, properties and uses of a new class of materials. Mater Sci Eng 2000;28:1–63.
[6] Lee KM, Han CD. Polymer 2003;44:4573–88.
[7] Mitchell CA, Krishnamoorti R. Rheological properties of diblock copolymer/layered-silicate nanocomposites. J Polym Sci, Part B: Polym Phys 2002;40:1434–43.
[8] Krishnamoorti R, Yurekli K. Rheology of polymer layered silicate nanocomposites. Colloid Interface Sci 2001;6:464–70.
[9] Fornes TD, Yoon PJ, Keskkula H, Paul DR. Nylon 6 nanocomposites: the effect of matrix molecular weight. Polymer 2001;42:9929–40.
[10] Wagener R, Reisinger TJG. A rheological method to compare the degree of exfoliation of nanocomposites. Polymer 2003;44:7513–8.
[11] Reichert P, Hoffmann B, Bock T, Thomann R, Mulhaupt R, Friedrich C. Morphological stability of poly(propylene) nanocomposites. Macromol Rapid Commun 2001;22:519–23.
[12] Ray SS, Okamoto M. Polymer/layered silicate nanocomposites: a review from preparation to processing. Prog Polym Sci 2003.
[13] Ren J, Silva AS, Krishnamoorti R. Linear viscoelasticity of disordered polystyrene–polyisoprene block copolymer based layered-silicate nanocomposites. Macromolecules 2000;33:3739–46.
[14] Galgali G, Ramesh C, Lele A. A rheological study on the kinetics of hybrid formation in propylene nanocomposites. Macromolecules 2001;34:852–8.
[15] Hoffmann B, Dietrich C, Thomann R, Friedrich C, Mülhaupt R. Morphology and rheology of polystyrene nanocomposites based upon organoclay. Macromol Rapid Commun 2000;21:57–61.
[16] Lepoittevin B, et al. Poly(e-caprolactone)/clay nanocomposites prepared by melt intercalation: mechanical, thermal and rheological properties. Polymer 2002;43:4017–23.
[17] Ray SS, Okamoto M. Biodegradable polylactide and its nanocomposites: opening a new dimension for plastics and composites. Macromol Rapid Commun 2003;24:815–40.
[18] Zhao J. Rheological characterization of polystyrene–clay nanocomposites as the relate to the degree of exfoliation and dispersion. ANTEC 2003 [Chicago, IL].

[19] Morgan AB, Harris JD. Exfoliated polystyrene–clay nanocomposites synthesized by solvent blending with sonication. Polymer 2004;45: 8695–8703.
[20] Ferry JD. Viscoelastic properties of polymers. 3rd ed. New York: Wiley; 1980.
[21] Macosko CW. Rheology—principles, measurements, and applications. New York: Wiley; 1994.
[22] Garces JM. Private communication; 2003.